Algerian Journal of Engineering and Technology

Journal homepage: https://jetjournal.org/index.php/ajet

Original Article

Effects of absorber layer thickness and doping density on the performance of perovskite solar cells: a simulation analysis using SCAPS-1D software

Ibrahim Yaacoub Bouderbala* and Nor-El Houda Hamdi

Applied Optics laboratory, Institute of Optics and Precision Mechanics, University of Ferhat Abbas, Setif 19000, Algeria.

ARTICLE INFO

Article history:
Received 08 April 2023
Revised 11 June 2023
Accepted 14 June 2023

Keywords:
SCAPS-1D;
Perovskite solar cell;
$MASnI_3$;
Absorber layer;
Doping density.

ABSTRACT

The photovoltaic devices based on perovskite have witnessed a rapid increase in performance and are moving towards commercialization due to their low-cost electricity production. In this simulation work, we studied the photovoltaic performance of solar cells based on methylammonium tin iodide ($MASnI_3$) perovskite materials using the numerical simulation tool SCAPS-1D. The main objective is to improve the performance of this solar cell by determining the optimum properties for its operation. The influence of different key parameters, such as the thickness of the absorber layer and the doping acceptor density in the same layer, is thoroughly analyzed through SCAPS-1D. The optimized absorber layer with a thickness of 700 nm shows the highest power conversion efficiency of 26.21%. An increase in the doping density in the perovskite layer roughly increases the efficiency performance of the device to 30.21%. Based on our simulation results, it can be concluded that the TiO_2/$MASnI_3$/Spiro-OMeTAD structure for PSC is a potential alternative to the third generation of solar cells. It has the potential to be efficient and inexpensive in future research.

1. Introduction

With the relentless efforts of researchers in photovoltaics, several developing photovoltaic technologies have shown a growing interest in high optical and electrical performance, low-cost processes, and flexibility. Among these technologies, perovskite solar cells (PSCs) have recently emerged as one of the possible ways to achieve a low-cost and highly efficient solar cell, which has caught the attention of the renewable energy community. Perovskite, used as an absorber layer, has many advantages for solar cell devices, including a direct band gap, small exciton energy, long electron-hole diffusion, high light absorption, high tolerance to defects, and excellent bipolar carrier transport [1-4]. As a result of these properties, its power conversion efficiency (PCE) has increased from 3.2% [5] to 25.2% [6]. The perovskite material compounds have a crystal structure. The chemical formula of perovskite is ABX_3, where A represents an inorganic or organic cation, B represents an inorganic cation, and "X" is a halogen anion [7]. Despite the good performance of perovskite solar cells, there are some drawbacks that limit their applications and performance, such as the instability of the perovskite layer in high humidity conditions.

The most common absorber material used for PSCs is methylammonium (MA: CH_3NH_3) lead trihalide ($MAPbX_3$). The bandgap of $MAPbX_3$ usually falls within the range of 1.5–2.3 eV. Methylammonium lead iodide ($MAPbI_3$) is a direct bandgap material with approximately 1.55 eV, while methylammonium lead bromide ($MAPbBr_3$) has a comparatively wider bandgap of 2.3 eV for an 800 nm absorption onset. Formamidinium lead iodide ($FAPbI_3$) exhibits a narrower bandgap of 1.48 eV, indicating larger current but lower stability. Lead (Pb)-based perovskites

* *Corresponding author*. Tel.: +213 698 522 490
E-mail address: bouderbala.iy@hotmail.com
Peer review under responsibility of University of El Oued.
 https://doi.org/10.57056/ajet.v8i1.101

have been extensively studied and have shown promising results in various applications, particularly in solar cells. However, the presence of lead raises concerns due to its toxicity, which has prompted researchers to explore alternative materials. One such alternative is tin (Sn)-based perovskites, which have gained attention as potential replacements for lead-based perovskites. Sn-based perovskites have similar structural and electronic properties to Pb-based perovskites, making them attractive candidates. They offer the advantage of being environmentally friendly and less toxic than lead-based counterparts. In comparison to $MAPbI_3$, the perovskite layer of methylammonium tin iodide ($MASnI_3$) has not been explored as extensively. Both perovskite compounds have a tetragonal structure, even with different temperature processing, leading to different optical properties. Experimental data indicate that $MASnI_3$ serves as an excellent hole transporter with an absorption onset of 1.1 eV [8]. However, it is true that Sn-based perovskites have faced challenges in terms of stability compared to Pb-based perovskites. Sn-based perovskites tend to be more prone to degradation and have lower long-term stability, especially under exposure to heat, humidity, and light. This instability can lead to performance degradation and limit their practical applications [9]. Researchers are actively working to overcome these stability issues associated with Sn-based perovskites. Various strategies, such as compositional engineering, interface engineering, and encapsulation techniques, are being explored to enhance their stability and improve their performance [10-12].

A typical PSC structure generally consists of an electron transport layer (ETL) covered with a perovskite layer as the absorber (active layer), followed by a hole transport layer (HTL). The morphology of the ETL and HTL influences the stability and efficiency of the PSCs. The photo-generated carriers pass through these layers before being collected. The typical device configuration is glass/transparent-conductive-oxide(TCO)/ETL/perovskite/-HTL/metal electrode.

Most research on PSCs focuses on perovskite deposition parameters. However, interpreting the results has not been easy. The main reason is the lack of established theoretical models and available data on layer parameters. Therefore, it is essential to utilize simulation software and numerical models to achieve better performance of solar cells by understanding the underlying mechanisms that hinder the optimum performance of PSC devices [13].

In this paper, we conducted numerical modeling and simulation of lead-free PSCs using perovskite-$CH_3NH_3SnI_3$ ($MASnI_3$) to develop a non-toxic, highly efficient, and stable PSC. We employed as the hole transport layer (HTL) 2,2',7,7'-Tetrakis[N,N-di(4-methoxyphenyl)amino]-9,9'-spirobifluorene (Spiro-OMeTAD) and Titanium dioxide (TiO_2) as the electron transport layer (ETL). For simulation purposes, we utilized SCAPS-1D (Solar Cell Capacitance Simulator), a one-dimensional simulation software developed by the University of Gent, Belgium. SCAPS-1D allows us to simulate the electrical characteristics of various types of solar cells, such as CZTS, CdTe, CIGS, by solving the basic semiconductor device equations under steady-state conditions. The software is based on the resolution of the continuous Poisson's differential equation [14]. By using the SCAPS-1D simulator, we confirmed that the lead-free, Sn-based perovskite solar cell exhibits high performance under both dark and illuminated conditions. The results demonstrate that our lead-free PSC, simulated with Sn-based perovskite instead of Pb-based perovskite, achieves a theoretical efficiency as high as 30.21%.

2. Materials and Methods

To simulate the performance of PSCs using different thicknesses and band gap energies of the tin-based perovskite layer, we utilized SCAPS-1D software version 3.3.08 (ELIS, University of Gent, Belgium) [15]. The simulation was conducted at a working temperature of 300 K under AM 1.5 G 1 sun illumination. The proposed structure of the PSC is depicted in Fig. 1.

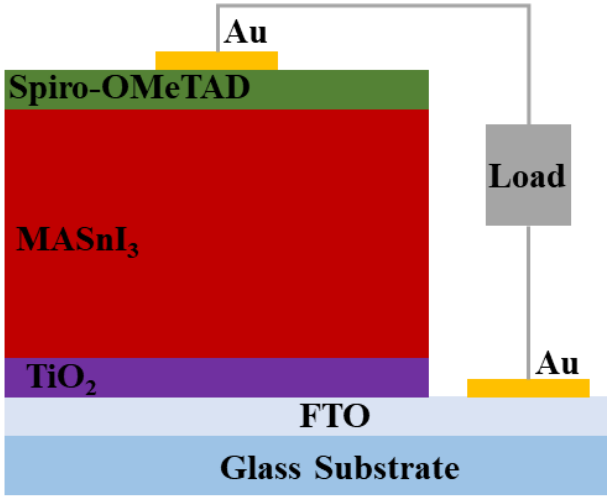

Fig 1. Perovskite solar cell structural design.

Our study employed a planar structure composed of five layers: FTO/TiO_2/$MASnI_3$/Spiro-OMeTAD/Au. FTO serves as the transparent conductive oxide (TCO) with a bandgap of 4.4 eV, while Au functions as the counter electrode. The absorber layer's parameters were adjusted in order to optimize the performance of the solar cell and achieve maximum photovoltaic efficiency. In all device configurations, $MASnI_3$ was positioned as an intermediate

layer between the electron extractor (TiO_2) and the hole extractor (Spiro-OMeTAD). The cell structure is illustrated in Fig. 1. All the physical parameters required for the simulation were gathered from reported research papers and experimental data, and their respective values are presented in Table 1.

Table 1. The semiconductor parameters of the PSC's components used in the simulation.

Term	**Parameter**	**TCO [16, 17]**	**TiO_2 [18, 19]**	**$MASnI_3$ [20]**	**Spiro-OMeTAD [21-23]**
Thickness	d (nm)	500	100	300	100
Band gap	E_g (eV)	3.5	3.2	1.3	3.17
Affinity	χ (eV)	4	4.26	4.2	2.2
Permittivity	ε_r	9	9	8.2	3
Effective density of states at CB	N_C (cm^{-3})	2.20×10^{18}	2.00×10^{18}	1.00×10^{18}	2.50×10^{18}
Effective density of states at VB	N_V (cm^{-3})	1.80×10^{19}	1.80×10^{19}	1.00×10^{18}	1.80×10^{19}
Electron thermal velocity	(cm/s)	1.00×10^{7}	1.00×10^{7}	1.00×10^{7}	1.00×10^{7}
hole thermal velocity	(cm/s)	1.00×10^{7}	1.00×10^{7}	1.00×10^{7}	1.00×10^{7}
Mobility of electrons	μ_n (cm^2/V.s)	20	20	1.6	2.00×10^{-4}
Mobility of holes	μ_p (cm^2/V.s)	10	10	1.6	2.00×10^{-4}
Density of n-type doping (donor)	N_D (cm^{-3})	2.00×10^{19}	6.00×10^{19}	/	/
Density of p-type doping (Acceptor)	N_A (cm^{-3})		/	1.00×10^{14}	2.00×10^{19}
Density of defects	N_t (cm^{-3})	1.00×10^{15}	1.00×10^{15}	2.50×10^{13}	1.00×10^{15}

The interface parameters are provided in Table 2. The simulation parameters were initially set to establish a base configuration. Subsequently, various properties of the perovskite solar cell were modified to investigate their effects on the device performance and achieve an optimized outcome. For achieving a high-power conversion efficiency (PCE), an initial thickness of 100 nm was assigned to the Spiro-OMeTAD and TiO_2 layers, while a thickness of 300 nm was designated for the $MASnI_3$ layer, as indicated in Table 1.

By utilizing the SCAPS-1D software, we are able to incorporate defect layers at the interfaces. Table 2 summarizes the defect density introduced at each of the TiO_2/$MASnI_3$ and $MASnI_3$/Spiro-OMeTAD interfaces.

Table 2. Defect density values inside the layers.

Parameters \ Interface	**TiO_2 /$MASnI_3$ [24]**	**$MASnI_3$/Spiro-OMeTAD [24]**
Defect Type	Neutral	Neutral
Capture cross section for electrons $\boldsymbol{\sigma_n}$ (cm^{-2})	1.00×10^{-17}	1.00×10^{-18}
Capture cross section for hole $\boldsymbol{\sigma_p}$ (cm^{-2})	1.00×10^{-18}	1.00×10^{-19}
Energetic distribution	Single	Single
Energy level with respect to Ev (eV)	0.6	0.6
Characteristic energy (eV)	0.1	0.1
Total density $\boldsymbol{N_t}$ (cm^{-3})	1.00×10^{9}	1.00×10^{9}

3. Results and discussion

The simulation was conducted at a working temperature of 300 K under AM 1.5 G 1 sun illumination. The energy band diagram, as depicted in Fig. 2a, was obtained from SCAPS-1D to analyze the optical properties of the PSC. The band gap of the Spiro-MeOTAD buffer layer was adjusted in conjunction with the $MASnI_3$ absorber and TiO_2 window layers. To maximize light absorption, the absorber layer should have a band gap equal to or greater than 1.3 eV, which aligns with the band gap of our absorber layer.

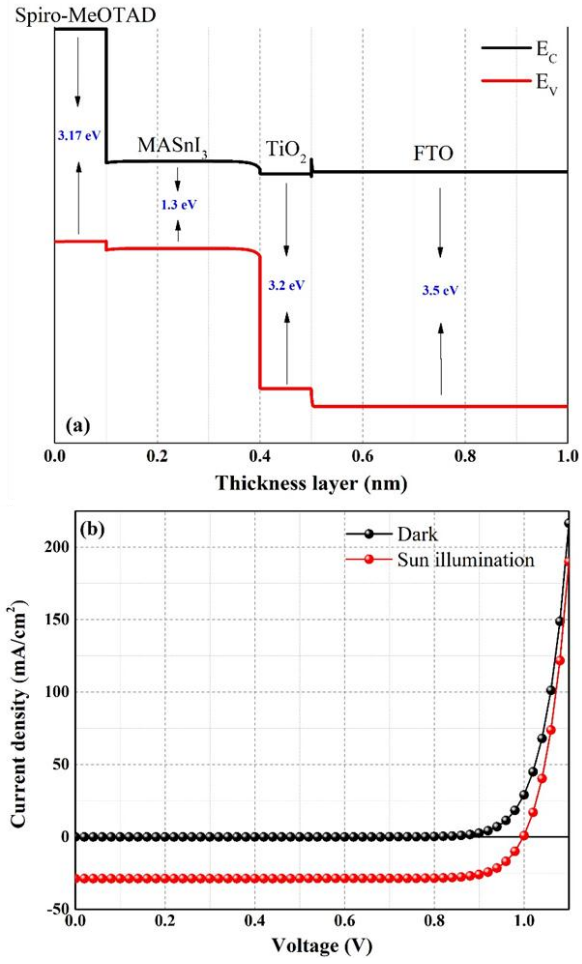

Fig 2. (a) Energy Band Diagram and (b) J–V Curve under dark and sun illumination

Fig. 2b represents the I-V curve of the PSC under both dark and sunlight conditions. We obtained an open circuit voltage (V_{OC}) of 0.99 V, a short circuit current density (J_{SC}) of 28.74 mA/cm^2, a fill factor of 82.99%, and an efficiency of 23.82%. To examine the impact of layer thickness (ETL, HTL, and perovskite) on the PSC performance, we initially varied the thicknesses of the Spiro-OMeTAD and TiO_2 layers from 50 nm to 350 nm with a fixed step of 50 nm. Interestingly, the performance parameters of all the device configurations exhibited similar results when the hole transport material (HTM) was varied, with only marginal changes observed in the fill factor (*FF*) and open circuit voltage (V_{OC}). Additionally, slight variations were observed in the graph curves of current density and the energy band diagram. Consequently, the changes in ETL and HTL thicknesses did not significantly affect the parameters of all-PSCs and can be disregarded. Therefore, we maintained the ETL and HTL thickness at 100 nm, as it did not result in any substantial changes in the performance parameters.

To examine the impact of the thickness of the perovskite absorber layer on the solar cell's performance, the thickness was varied from 0.3 µm to 2.5 µm. As the thickness increased, the J-V characteristics curve shifted away from the origin, as we can see by the changing in values from Table 3. The effect of thickness on the P-V characteristics curves is also evident in Fig. 2b. It is noteworthy that increasing the thickness of the absorber layer improves the power density of the cell. This is because a greater thickness of the absorber layer increases the likelihood of capturing photons, resulting in a higher conversion of solar power into electrical power density.

The thickness of the absorber layer was varied from 0.3 µm to 2.0 µm, and it was observed that the J-V characteristics curve shifted away from the origin, as depicted in Fig. 2a. The PSC parameters corresponding to the increase in absorber layer thickness are presented in Table 3. It is known that a thin absorber layer results in low photogenerated current, as evidenced by the case when 300 nm thickness was used. However, the charge extraction is high, as indicated by the high V_{OC}, which suggests reduced recombination.

Table 3. Performance parameters of PSC device with various thicknesses of the absorber layer.

Thickness (nm)	V_{OC} *(V)*	J_{SC} *(mA/cm^2)*	*FF %*	*PCE %*
300	0.998	28.74	82.99	23.82
400	0.986	31.06	82.50	25.28
500	0.976	32.43	81.93	25.95
600	0.968	33.28	81.31	26.19
700	0.960	33.83	80.64	26.21
800	0.954	34.20	79.96	26.09
900	0.948	34.45	79.25	25.89
1000	0.943	34.63	78.53	25.64
1100	0.938	34.75	77.80	25.37
1200	0.933	34.84	77.07	25.08
1300	0.929	34.91	76.34	24.78
1400	0.926	34.96	75.59	24.48
1500	0.923	34.99	74.83	24.17
1600	0.920	35.02	74.06	23.86
1700	0.917	35.04	73.29	23.55
1800	0.914	35.047	72.51	23.23
1900	0.911	35.053	71.70	22.91
2000	0.909	35.057	70.88	22.59

The impact of thickness on the P-V characteristics curves is evident from Table 3. As indicated in the table, J_{SC} increases with thickness, resulting in improved light absorption. Specifically, it increases from 28.74 to

34.63 mA/cm^2 as the thickness is increased from 300 nm to 1000 nm. Beyond this thickness, J_{SC} continues to increase but with a lower rate until it saturates at around 35mA/cm^2. It is worth noting that at a thickness of 300 nm, JSC is comparatively lower than the other values due to the reduced absorption of long-wavelength photons [25].

By increasing the thickness of the absorber layer, the effective band gap decreases, allowing for the absorption of long wavelength photons [26]. This increase in thickness results in a higher number of photons being captured, thereby converting more solar power into electrical power density. Based on our findings, an absorber thickness of 600-700 nm is considered optimal. At a thickness of 700 nm, the power efficiency reached the highest value among the different thicknesses at 26.21%. We observe an efficiency improvement of approximately 2.4% when increasing the thickness from 300 nm to 700 nm.

Beyond 700 nm, the cell efficiency continues to decrease due to the maximum absorption of light, as indicated by the nearly constant J_{SC} values. Additionally, when the thickness of the absorber layer exceeds the diffusion length, the charge carriers generated near the center of the layer will recombine. Our study demonstrates that adjusting the perovskite absorber thickness to 600-700 nm can achieve high efficiency in PSCs.

Fig. 3 and Table 4 present the PSC parameters obtained for different acceptor doping densities in the perovskite layer, ranging from 1.00 × 10^{14} cm^{-3} to 1 × 10^{18} cm^{-3} [27].

Table 4. Performance parameters of PSC device with various doping concentration of the absorber layer.

Doping density (cm^{-3})	V_{OC} (V)	J_{SC} (mA/cm^2)	FF %	PCE %
1.00E+14	0.960	33.83	80.64	26.21
5.00E+14	0.961	33.84	81.45	26.49
1.00E+15	0.962	33.85	82.32	26.82
5.00E+15	0.978	33.82	83.90	27.75
1.00E+16	0.991	33.67	84.10	28.06
5.00E+16	1.028	32.93	84.76	28.69
1.00E+17	1.045	32.53	85.22	28.98
5.00E+17	1.086	31.73	86.39	29.79
1.00E+18	1.107	31.49	86.63	30.21

The effect of doping density concentration on PSC performance was studied and is illustrated in Fig. 3. It is observed that a high doping value increases Auger recombination. Therefore, the maximum doping concentration was fixed at 10^{18} cm^{-3}. By doping the absorber layer, impurities are introduced to create electron deficiencies or "holes" in the semiconductor material, which act as majority charge carriers. As the doping concentration increases, the number of available holes also increases, resulting in an enhanced mobility of charge carriers. Based on our results, we observed that the short-circuit current density increases with an increase in doping concentration. As the doping concentration increases from 10^{14}, the built-in electric field across the device also increases, enhancing the separation of the photogenerated carriers and resulting in higher V_{OC} and cell efficiency [28].

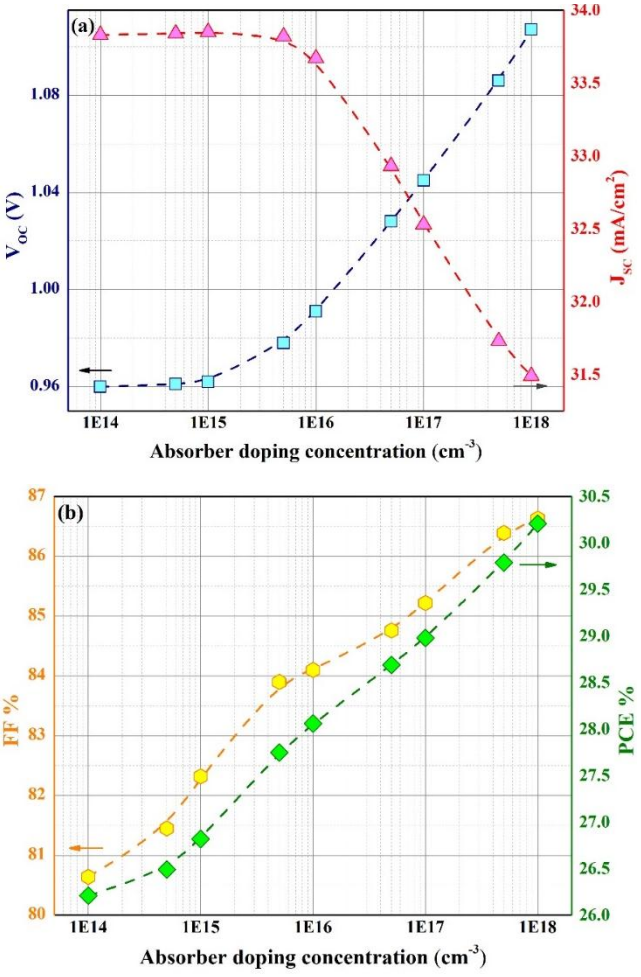

Fig 3. Influence of $MASnI_3$ thickness, (a) J_{SC} and V_{OC}, (b) Fill factor and efficiency.

Our study's results have been compared to those of other relevant studies, and the findings are presented in Table 5.

Table 5. Comparison between our results and those of others

	Perovskite structure	V_{OC} (V)	J_{SC} (mA/cm^2)	FF %	PCE %
Our results	**FTO/TiO_2/$MASnI_3$/Spiro-OMeTAD/Au**	**1.11**	**31.49**	**86.63**	**30.21**
Mandadapu et *al.*, [29]	TiO_2/ZnO:Al/$MASnI_3$/CuI/Au	1.04	31.77	78.18	25.91
Husainat et *al.*, [15]	FTO/TiO_2/$MAPbI_3$/Spiro-OMeTAD/Au	1.47	22.65	91.00	20.34
Azri et *al.*, [30]	ITO/ZnO/$MAPbI_3$/ CuSCN /Au	1.27	21.89	83.70	23.30
Abdelaziz et *al.*, [31]	FTO/ZnO/$FASnI_3$/Spiro-OMeTAD/Au	0.92	22.65	76.74	14.03
Yasin et *al.*, [32]	FTO/$MASnCl_3$/$MASnI_3$/$MASnI_3$/Au	1.00	28.11	87.69	24.81
Belarbi et *al.*, [33]	FTO/ZnO /$MAPbI_3$/PEDOT: PSS/ITO	0.84	25.60	94.68	20.25
Gan et *al.*, [34]	FTO/ZnO/CsPbI3/FAPbI3/CuSCN/Au	1.31	26.11	83.78	28.75

Our research has yielded remarkable results, showcasing the exceptional efficiency of our structure and parameters compared to other. Through rigorous experimentation and analysis, we have consistently demonstrated a high performance. These findings confirm the efficacy of our approach and underscore its potential to revolutionize the field for real application.

4. Conclusion

In this work, planar type perovskite solar cell was simulated by using SCAPS-1D simulation program. Thickness and doping density of perovskite layer were varied to study their effects PSC properties. It was observed that device with when the absorber thickness is between 300 and 700 nm, cell efficiency improved from about 23% to 26.21%. Beyond 700 nm, JSC and cell efficiency increases more slowly and saturate at 1000 nm due to saturation in light energy absorption. We found that the suitable thickness of the absorber layer is between 600 and 700 nm and we don't need to use higher thickness. Moreover, it has been observed that the varying doping acceptor density of the perovskite layer has significant impact on the device operation and its performance. This is due the improved fill facto which can reduce sheet resistance of the absorber layer. The highest PSC that we obtained using SCAPS-1D simulation program was 30.21%.

Conflict of Interest

Authors are required to disclose financial or non-financial interests that are directly or indirectly related to the work submitted for publication.

References

1. Wang Z, Lin Q, Chmiel FP, Sakai N, Herz LM, Snaith HJ. Efficient ambient-air-stable solar cells with 2D–3D heterostructured butylammonium-caesium-formamidinium lead halide perovskites. *Nature Energy*. 2017, 2;9:1-10.
2. Liu Y, Yang, Z, Cui D, Ren X, Sun J, Liu X, Zhang J, Wei Q, Fan H, Yu F, Zhang X, Zhao C, Liu S. Two- inch- sized perovskite CH3NH3PbX3 (X= Cl, Br, I) crystals: growth and characterization. *Advanced materials*. 2015, 27;35:5176-5183.
3. Yang D, Yang Z, Qin, W, Zhang Y, Liu SF, Li C. Alternating precursor layer deposition for highly stable perovskite films towards efficient solar cells using vacuum deposition. *Journal of Materials Chemistry A*. 2015, 3;18:9401-9405.
4. Lin Q, Armin A, Nagiri RCR, Burn PL, Meredith P. Electro-optics of perovskite solar cells. *Nature Photonics*. 2015, 9;2:106-112.
5. Kojima A, Teshima K, Shirai Y, Miyasaka T. Organometal halide perovskites as visible-light sensitizers for photovoltaic cells. *Journal of the american chemical society*. 2009, 131;17:6050-6051.
6. "NREL Efficiency Chart 2021," https://www.nrel.gov/pv/cell-efficiency.html, Apr.2022.
7. Atta NF, Galal A, El-Ads EH, Tech. Chapter 4, 2016, 108-151.
8. Heo JH, ImSH, Noh JH, Mandal TN, Lim CS, Chang JA, Lee YH, Kim H, Sarkar A, Nazeeruddin MK, Grätzel M, Seok SI. Efficient inorganic–organic hybrid heterojunction solar cells containing perovskite compound and polymeric hole conductors. *Nature photonics*. 2013, 7;6:486-491.
9. Hussein M, Iqbal Z, Li G, Pascual J, Alharthi F, Abate A, Li M, Challenges in tin perovskite solar cells. *Phys. Chem. Chem. Phys*. 2021, 23;41:23413-23427.
10. Prakash J, Singh A, Sathiyan G, Ranjan R, Singh A, Garg A, Gupta RK. Progress in tailoring perovskite based solar cells through compositional engineering: Materials properties, photovoltaic performance and critical issues. *Materials today energy*. 2018, 9:440-486.
11. Ran C, Xi J, Gao W, Yuan F, Lei T, Jiao B, Hou X, Wu Z. Bilateral interface engineering toward efficient 2D–3D bulk heterojunction tin halide lead-free perovskite solar cells. *ACS Energy Letters*. 2018, 3;3:713-721.

12. Li B, Chang B, Pan L, Li Z, Fu L, He Z, Yin L. Tin-based defects and passivation strategies in tin-related perovskite solar cells. *ACS Energy Letters*. 2020, 5;12:3752-3772.
13. Eli D, Onimisi MY, Garba S, Ugbe RU, Owolabi JA, Ige OO, Ibeh GJ, Muhammed AO. Simulation and optimization of lead-based perovskite solar cells with cuprous oxide as a P-type inorganic layer. *Journal of the Nigerian Society of Physical Sciences*. 2019,1;2:72-81.
14. Hussain SS, Riaz S, Nowsherwan GA, Jahangir K, Raza A, Iqbal MJ, Sadiq I, Hussain SM, Naseem S. Numerical modeling and optimization of lead-free hybrid double perovskite solar cell by using SCAPS-1D. *Journal of Renewable Energy*. 2021, 1-12.
15. Burgelman M, Nollet P, Degrave S. Modelling polycrystalline semiconductor solar cells. *Thin solid films*. 2000, 361:527-532.
16. Rutledge SA, Helmy AS. Carrier mobility enhancement in poly (3, 4-ethylenedioxythiophene)-poly (styrenesulfonate) having undergone rapid thermal annealing. *Journal of Applied Physics*. 2013, 114;13:133708.
17. Jayan KD, Sebastian V. Comprehensive device modelling and performance analysis of $MASnI_3$ based perovskite solar cells with diverse ETM, HTM and back metal contacts. Solar Energy. 2012, 217:40-48.
18. Du HJ, Wang WC, Zhu JZ. Device simulation of lead-free $CH_3NH_3SnI_3$ perovskite solar cells with high efficiency. *Chinese Physics B*. 2016, 25;10:108802.
19. Husainat A, Ali W, Cofie P, Attia J, Fuller J. Simulation and analysis of methylammonium lead iodide ($CH_3NH_3PbI_3$) perovskite solar cell with Au contact using SCAPS 1D simulator. *American Journal of Optics and Photonics*. 2019,7;2:33.
20. Sahu A, Dixit A. Inverted structure perovskite solar cells: A theoretical study. *Current Applied Physics*. 2018,18;12:1583-1591.
21. Hao F, Stoumpos CC, Cao DH, Chang RP, Kanatzidis MG. Lead-free solid-state organic–inorganic halide perovskite solar cells. *Nature photonics*. 2014, 8;6:489-494.
22. Hock R, Mayer T, Jaegermann W. P-type doping of spiro-MeOTAD with WO_3 and the Spiro-MeOTAD/WO_3 interface investigated by synchrotron-induced photoelectron spectroscopy. *The Journal of Physical Chemistry C*. 2012, 116;34:18146-18154.
23. Mandadapu U, Vedanayakam SV, Thyagarajan K, Reddy MR, Babu BJ. Design and simulation of high efficiency tin halide perovskite solar cell. *Int. J. Renewable Energy Res*. 2017, 7;4:1603-1612.
24. Raoui Y, Ez-Zahraouy H, Tahiri N, El Bounagui O, Ahmad S, Kazim S. Performance analysis of $MAPbI_3$ based perovskite solar cells employing diverse charge selective contacts: Simulation study. *Solar Energy*. 2019,193:948-955.
25. Liu D, Gangishetty MK, Kelly TL. Effect of $CH_3NH_3PbI_3$ thickness on device efficiency in planar heterojunction perovskite solar cells. *Journal of Materials Chemistry A*. 2014, 2;46:19873-19881.
26. Pazos-Outón LM, Xiao TP, Yablonovitch E. Fundamental efficiency limit of lead iodide perovskite solar cells. *The journal of physical chemistry letters*. 2018, 9;7:1703-1711.
27. Singh AK, Srivastava S, Mahapatra A, Baral JK, Pradhan B. Performance optimization of lead free-$MASnI_3$ based solar cell with 27% efficiency by numerical simulation. *Optical Materials*. 2021, 117:111193.
28. Lin L, Li P, Jiang L, Kang Z, Yan Q, Xiong H, Lien S, Zhang P, Qiu Y. Boosting efficiency up to 25% for HTL-free carbon-based perovskite. *Sol. Energy*. 2021, 215:328–334.
29. Mandadapu U, Vedanayakam SV, Thyagarajan K, Babu BJ. Optimisation of high efficiency tin halide perovskite solar cells using SCAPS-1D. *International Journal of Simulation and Process Modelling*. 2018,13;3:221-227.
30. Azri F, Meftah A, Sengouga N, Meftah A. Electron and hole transport layers optimization by numerical simulation of a perovskite solar cell. *Solar energy*, 2019,181:372-378.
31. Abdelaziz S, Zekry A, Shaker A, Abouelatta M. Investigating the performance of formamidinium tin-based perovskite solar cell by SCAPS device simulation. *Optical Materials*. 2020,101:109738.
32. Yasin S, Al Zoubi T, Moustafa M. Design and simulation of high efficiency lead-free heterostructure perovskite solar cell using SCAPS-1D. *Optik*. 2021,229:166258.
33. Belarbi M, Zeggai O, Louhibi-Fasla S. Numerical study of methylammonium lead iodide perovskite solar cells using SCAPS-1D simulation program. *Materials Today: Proceedings*, 2022,51:2115-2119.
34. Gan Y, Zhao D, Qin B, Bi X, Liu Y, Ning W, Yang R, Jiang, Q. Numerical Simulation of High-Performance $CsPbI_3$/$FAPbI_3$ Heterojunction Perovskite Solar Cells. *Energies*, 2022,15;19:7301.

Recommended Citation

Bouderbala IY, Hamdi N. Effects of absorber layer thickness and doping density on the performance of perovskite solar cells: a simulation analysis using SCAPS-1D software. *Alger. J. Eng. Technol. 2023*;8(1):131-137. https://doi.org/10.57056/ajet.v8i1.101